ADVANCED ENERGY MATERIALS
www.advenergymat.de

Screen-Printable Thin Film Supercapacitor Device Utilizing Graphene/Polyaniline Inks

Yanfei Xu, Matthias Georg Schwab, Andrew James Strudwick, Ingolf Hennig, Xinliang Feng, Zhongshuai Wu, and Klaus Müllen**

The current development trend towards miniaturized portable electronic devices has raised the demand for rechargeable power sources of appropriate size.[1] In addition, future developments are aiming at thin, light, cheap, flexible and sustainable solutions, with wearable electronics as one typical application. More specifically, the emerging field of "printed electronics",[2] including printable transistors,[3] solar cells,[4] and organic light emitting diodes[5] has the potential to meet these goals in future applications. However, a compatible energy source for these applications is still lacking. Fully printable charge storage devices show great promise for allowing the full integration into the manufacturing process of printed electronics.

Conventional charge storage devices such as batteries are often limited by their bulkiness, low power density, low charge-discharge rates, and are frequently the expensive components of electronic devices.[6] Supercapacitors are unique electrochemical energy storage devices with complementary properties to Li-ion batteries, and are considered promising candidates for alternative energy storage devices as a result of their pulse power supply, long cycle life, and low maintenance cost.[7,8]

To realize the printable potential for supercapacitor on an industrial scale, an inexpensive process for producing the thin film electrodes is required. Typically, one of the most important and powerful industrial printing techniques for the thin film fabrication is screen-printing, which is inexpensive, rapid, and capable of mass production.[5,9] Furthermore, screen printing allows for good control over the deposition area, and the ink can be printed on a wide variety of substrates, including paper, fabrics, plastics, etc.[10] Since the performance of screen-printed supercapacitor is strongly governed by the ink that is applied to the process, thus, it is necessary to explore ideal materials for the functional ink formulation.

Graphene-based materials are promising candidates for supercapacitors,[11–13] owing to the high electrical conductivity,[14,15] large specific surface area,[16] flexibility[17] as well as high mechanical strength and chemical stability.[18] Recently, Jang and co-workers produced curved nano graphene platelets (NGP) by oxidation of graphite according to a modified Hummers' method and a subsequent thermal shock exposure exfoliation method.[19–21] Within a reasonable range of oxygen functional group content in NGP, the dispersibility, large specific surface area and high conductivity of these NGP are generally coexisting.[19–22] Furthermore, it is exciting that the specific capacitances of NGP based supercapacitor in ionic liquid electrolyte are 100–250 F g^{-1}, with energy density of 85.6 Wh kg^{-1} compared to the previous result of 28.5 Wh kg^{-1} obtained elsewhere using standard graphene materials produced via the hydrazine reduction of graphene oxide.[19,23] These results strengthen the suggestion that NGP material will be a promising candidate for futher industrial ink formulation and supercapacitor application.

Polyaniline (PANI) is another highly promising electrode material for supercapacitors due to its high pseudocapacitance. The pseudocapacitance originates from the PANI undergoing fast and reversible faradic redox reactions.[11] However, one of the drawbacks for PANI as supercapacitor electrodes is it's poor cycling stability because PANI is usually brittle and weak in mechanical strengths. Additionally, PANI exhibits only moderate electrical conductivity.[24] To overcome these PANI drawbacks, graphene has been used as an excellent substrate to host active polymer nanomaterial.[25–27] NGP can serve as a stable and underlying conductive network for the PANI when combining the NGP and PANI together. At the same time, the PANI can serve as spacer to further separate NGP neighboring sheets, and PANI can also enhance the final capacity through fast faradaic pseudocapacitance effects. Therefore, high capacitances and improved stability is expected to be achieved with NGP/PANI hybrid materials. Thus, it is attractive to formulate the industrial NGP/PANI inks to harness these synergistic capacitive properties.

In this work, we formulate a series of NGP/PANI inks with different weight ratios ranging from 1:0 to 1:0.5, 1:1, 1:1.5 and 1:2 (labeled as NGP, NGP/$PANI_{1:0.5}$, NGP/$PANI_{1:1}$, NGP/$PANI_{1:1.5}$, NGP/$PANI_{1:2}$, more ink formulation details are given in the experimental part), and demonstrate their industrial applicability to the fabrication of supercapacitor electrodes by screen printing techniques. With these NGP/PANI thin films, two-electrode supercapacitor test cells are fabricated as these devices best represent those commonly produced commercially. The electrochemical properties of the supercapacitors are investigated by means of cyclic voltammetry (CV), galvanostatic charge discharge and impedance spectroscopy techniques.

The key issues to address for the successful industrial exploitation of ink formulation are: ensuring large-scale and

Dr. Y. Xu, Dr. M. G. Schwab, Dr. A. J. Strudwick
Carbon Materials Innovation Center
GVM/I, BASF SE, 67056 Ludwigshafen, Germany
E-mail: yanfeixu103@gmail.com
Dr. I. Hennig
GMC/R, BASF SE, 67056 Ludwigshafen, Germany
Dr. X. Feng, Dr. Z. Wu, Prof. K. Müllen
Max-Planck-Institut für Polymerforschung
55128 Mainz, Germany
E-mail: muellen@mpip-mainz.mpg.de

DOI: 10.1002/aenm.201300184

cost-reasonable production methods, whilst providing a balance between ease of fabrication and final ink quality. In order to avoid any contamination of the ink and the electrodes prepared thereof with metal impurities from the ball milling step, electrochemical inert beads (ZrO_2 68%/SiO_2 32%) are applied.

The NGP X-ray diffraction (XRD) (Figure S1A, supporting information) spectra shows low intensity, broad diffraction peak appears at 2θ of 24.5 ~ 27.5°, which can be indexed into the disorderedly stacked NGP sheets with a d-spacing of 0.339 nm, suggesting some degree of reaggregation of the exfoliated NGP sheets. The diffraction peak visible at 2θ of 10.0° is related to a corresponding d-spacing of 0.885 nm. The peak appearing at 2θ of 45° and 60° is possibly the (004) reflection of graphitic components originating from the starting material.[28] Scanning electron microscope (SEM) analysis confirms that the bulk NGP material is composed of rosette-type spherical particles which are composed of agglomerated carbon sheets (Figure S1B and Figure S1C). The agglomerates can be easily "unfolded" by applying liquid-assisted exfoliation procedures. Thus, results of transmission electron microscopy (TEM) characterization confirm that NGP material can be easily dispersed at the state of exfoliation by ball milling treatment in ethanol leading to a material that consists of exfoliated, crumpled graphene sheets (Figure S1D).

To determine the chemical composition of NGP, X-ray photoelectron spectroscopy (XPS) measurements are carried out in the region of 0 ~ 1300 eV (Figure S1E). The XPS confirm that, apart from the C=C peak at 284.6 eV, the C–C peak at 285.2 eV, and the π–π* satellite peak at 291 eV, four other peaks can be deconvoluted, indicating the presence of other available oxygen containing functional groups, namely, hydroxyl (C–O at 285.7 eV), epoxy/ether (C–O–C at 286.2 eV), carbonyl (C = O at 287.5 eV), and carboxylate (O–C=O at 289.4 eV) (Figure S1F).[29]

Next, we turn to the description of the screen printing process used for the fabrication of supercapacitor electrode. Thin and homogeneous films are not easily obtained by screen printing. The quality of screen-printed thin films depends highly on printing conditions including printing speed, ink stability and especially ink viscosity. The viscosity performance of the inks as a function of the applied shear rate is shown in Figure S2. The NGP/PANI inks used herein all exhibit good shear thinning behavior with a viscosity of around 125 mPa.s observed at a shear rate of 10 s^{-1}. From these viscosity results we conclude that the formulation used in this work fits the screen-printing requirements.[30]

Figure 1 illustrates the screen printing method that is applied in this study. During deposition, the screen is placed a few millimeters above the surface of the substrate (Figure 1A). After loading the NGP/PANI ink onto the screen, a rubber squeegee is swept with a velocity of 35 cm s^{-1} across the surface of the screen (Figure 1B and Figure 1E) thus bringing it into close contact with the substrate. At this point, the ink flows from the screen to the surface of the substrate. As the squeegee passes over a region, the screen separates from the substrate, leaving behind ink that dries to yield a continuous film (Figure 1C and 1D).

In addition, when compared with other plastic substrates, carbon fabric substrates dramatically improve film adhesion and simplify the coating process due to the fibrous paper-like

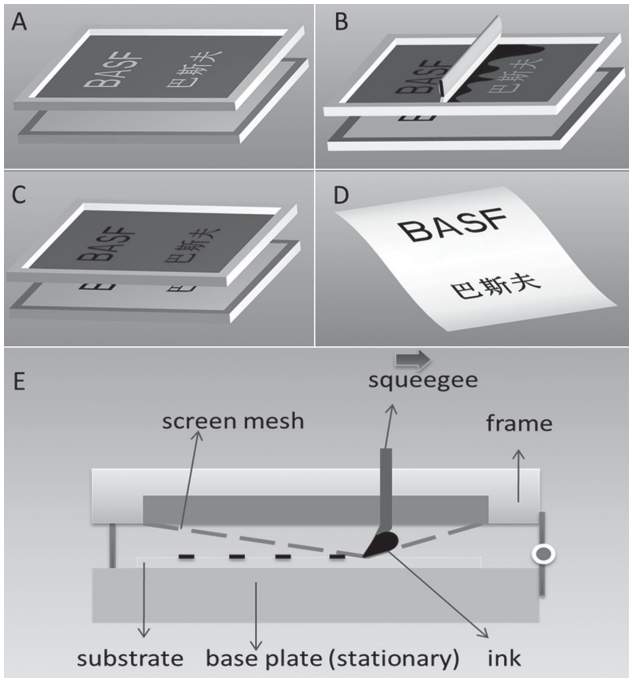

Figure 1. Schematic illustration of the screen-printing process. The thin film thickness is controlled by the screen mesh, speed of the squeegee and ink. The NGP/PANI dry thin film thickness (measured on PET) typically ranges from 5 to 15 μm.

structure of the material. Moreover, as the carbon fabric substrates are electrically conductive, NGP/PANI thin films printed on these substrates can be used as electrodes for the supercapacitor directly. Figure S3 shows optical photographs screen printed NGP/$PANI_{1:1.5}$ thin films on a hard carbon fabric substrate, a soft carbon substrate and the supercapacitor electrodes prepared thereof. The NGP/PANI dry thin film thickness typically ranges from 5 to 15 μm. The well-defined area of NGP/$PANI_{1:1.5}$ coating is achieved by the mask to protect the uncoated area. A thin film with dimensions of 4 cm × 3 cm shown in Figure S3 can be fabricated in a short timescale of 0.1 seconds. The ability to produce thin films of high quality on this short timescale is highly desirable in industrial applications.

Raman spectroscopy (Figure S4) is used to study the surface compositions of the NGP and NGP/PANI films. NGP shows two distinctive peaks centered at ~1363 cm^{-1} and ~1590 cm^{-1} that correspond to D and G bands, respectively. Three new representative peaks arising from PANI can be indexed at 1184, 1234, 1508 cm^{-1}, apart from the D/G bands of graphene. They correspond to the C–H bending vibration of benzenoid rings, C–N stretching vibration of benzenoid rings, and stretching vibrating of C=N in quinonoid ring systems of PANI.[31]

SEM images of the carbon fabric substrate, NGP and NGP/$PANI_{1:1.5}$ films are shown in **Figure 2**A–F. Figure 2A, 2B show an SEM surface image of the morphology of the hard carbon fabric substrate. The rough surface is advantageous for energy storage devices due to enhanced electrolyte access to and its intimate interaction with the electrode material; Figure 2C shows low-magnification SEM of the screen-printed NGP

Adv. Energy Mater. 2013,
DOI: 10.1002/aenm.201300184

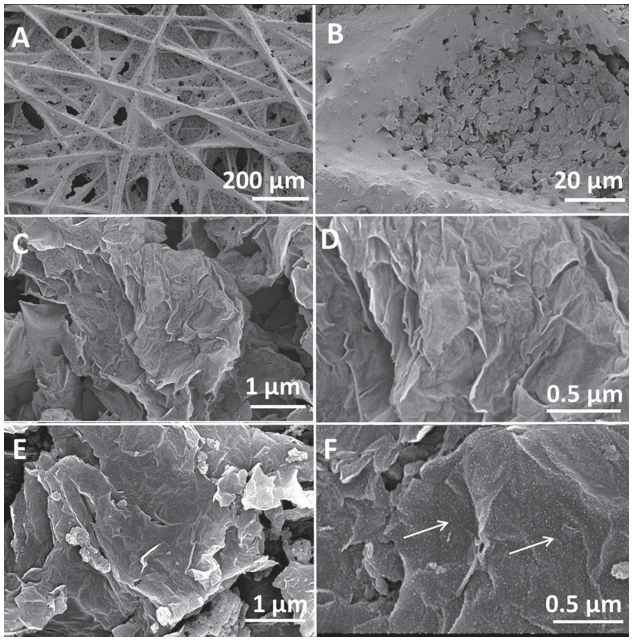

Figure 2. A,B) SEM images of the carbon fabric substrate; C,D) NGP and E,F) NGP/PANI$_{1:1.5}$. Figure 2A, 2C, 2E show low-magnification SEM images. Figure 2B, 2D, 2F show high-magnification SEM images, the morphology of NGP and NGP/PANI sheets.

network which appears rough and porous. Figure 2D shows the curved NGP surface. As seen from images in Figure 2F (NGP/PANI$_{1:1.5}$), the small-compact PANI nanoparticles are homogeneously coated on the NGP sheet, keeping the advantage of the entangled network of the NGP that also promotes good access of the electrolyte to the active PANI material. PANI is likely to be adsorbed onto the surface of graphene by π–π stacking.[32] The SEM images for the other NGP/PANI films are shown in the Figure S5.

Nitrogen adsorption–desorption analysis is used to determine the Brunauer-Emmett-Teller (BET) specific surface area of the NGP, NGP/PANI$_{1:0.5}$, NGP/PANI$_{1:1}$, NGP/PANI$_{1:1.5}$ and NGP/PANI$_{1:2}$ materials. The corresponding values are 497, 260, 232, 215, 184 m^2 g^{-1}, while the specific surface area for the carbon substrate and pure PANI is only 2 and 34 m^2 g^{-1}. The electrical conductivity of the corresponding films are 8.4, 1.2, 0.28, 0.13 and 0.31 S cm^{-1}, respectively. These results show that with increasing NGP content, the electrode composites show an increase of specific surface area and conductivity.[25]

The electrochemical performances of the series of screen-printed NGP/PANI electrodes are analyzed by using CV in 1.0 M aqueous H_2SO_4 electrolyte within a potential window from –0.2 to 0.8 V vs. saturated calomel electrode (SCE), using a three-electrode system. The NGP/PANI ink is directly screen printed on the hard carbon substrate and used as working electrodes with a diameter of ~ 2 cm (Figure S3C). **Figure 3**A shows the CV results of different NGP/PANI electrodes at a scan rate of 20 mV s^{-1}, which demonstrates that all NGP/PANI electrodes reveal a larger capacitive response than the pure NGP electrode itself. The redox peaks (a1/a2, b1/b2) of NGP/PANI films shown in Figure 3A are attributed to the redox transition of PANI, corresponding to its leucoemeraldine/emeraldine and emeraldine/pernigraniline structural conversions, respectively.[33,34] This observation additionally confirms the presence of pseudocapacitive PANI in the electrodes. The origin of the observed c1/c2 peaks is as yet unknown, one possible explanation is that they are related to the redox peaks originating from the oxygenated groups of NGP.[25,35]

The potential position of NGP/PANI CV changes upon varying the mass ratios. A similar effect has been observed previously where the synergistic effect resulting from the interactions of PANI and NGP has been demonstrated to affect the potential position of CV curves.[34] A key result is the NGP/PANI$_{1:1.5}$ exhibiting a much higher current density than other NGP/PANI electrodes. Such electrochemical properties indicate that NGP/PANI$_{1:1.5}$ is the most promising material for use in supercapacitor electrodes of this type.[36] Figure 3B shows the CV results of NGP/PANI$_{1:1.5}$ obtained at different scan rates. With an increase of the scan rate, the redox current peaks increase, suggesting a surface-controlled electrochemical process.[37] Figure S6 shows CV results of other NGP/PANI and NGP electrodes at different scan rates, using a three-electrode system.

It should be noted that a three-electrode cell is valuable for quickly determining material electrochemical characteristics whereas a two-electrode cell shows the physical configuration, internal voltages and charge transfer that occurs in a packaged supercapacitor and thus provides the best indication of an electrode performance for industrial applications.[38] Therefore, symmetric, industry-level, two-electrode capacitors are built with a glass microfiber separator using a sandwich type construction (electrode/separator/electrode), in 1.0 M aqueous H_2SO_4 electrolyte. Here the NGP/PANI film is used as active electrode, and the carbon fabric substrate serves as current collector. The electrochemical behavior of the supercapacitor is investigated by CV (Figure 3C). The specific capacitance is calculated based on the integrated area of discharge CV curves yielding an average discharge current. At a scan rate of 20 mV s^{-1}, NGP, NGP/PANI$_{1:0.5}$, NGP/PANI$_{1:1}$, NGP/PANI$_{1:1.5}$ and NGP/PANI$_{1:2}$ deliver specific capacitances of 26, 85, 190, 269, and 177 F g^{-1}, based on the average active materials mass of one electrodes (including the mass of PTFE binder). Figure 3D shows the CV results of NGP/PANI$_{1:1.5}$ electrode obtained at different scan rates. There is a great increase in the current density at high scan rates, this demonstrates the good conductivity and the good capacitive behavior of NGP/PANI$_{1:1.5}$ electrode.[39] Figure S7 shows other NGP/PANI and NGP electrode CV results at different scan rates, using a two-electrode system. At a high scan rate of 100 mV s^{-1}, NGP, NGP/PANI$_{1:0.5}$, NGP/PANI$_{1:1}$, NGP/PANI$_{1:1.5}$ and NGP/PANI$_{1:2}$ deliver specific capacitances of 24, 83, 180, 236, and 150 F g^{-1} (Figure S8A). Again, the best capacitance performance is from the NGP/PANI$_{1:1.5}$ samples, which are consistent with the results obtained from the three-electrode system CV curves.

These optimal results observed for NGP/PANI$_{1:1.5}$ sample can be explained by the following reasons: first, since NGP provides a conductive host material for PANI,[40] thus, varying the NGP weight ratio within NGP/PANI films results in different interface morphology between NGP and PANI. The different morphologies are thought to significantly affect the formation

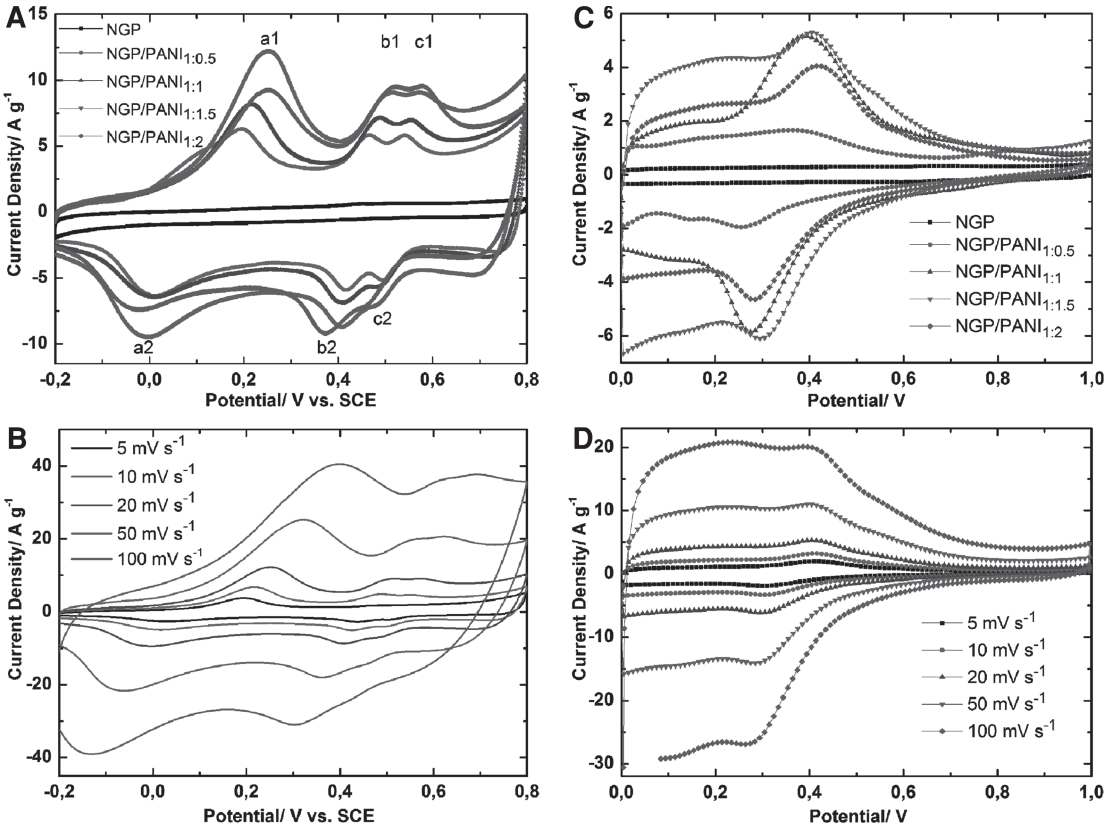

Figure 3. A) Electrochemical properties of the NGP, NGP/PANI electrodes measured at a scan rate of 20 mV s^{-1} in 1M H_2SO_4 electrolyte, three-electrode system. B) CV curves of the NGP/$PANI_{1:1.5}$ electrode from a scan rate of 5 to 100 mV s^{-1} in 1M H_2SO_4 electrolyte, three-electrode system. C) CV curves of NGP, NGP/PANI electrodes measured at a scan rate of 20 mV s^{-1}, in 1M H_2SO_4 electrolyte, two-electrode system. D) CV curves of NGP/$PANI_{1:1.5}$ electrode at different scan rates, in 1M H_2SO_4 electrolyte, two-electrode system.

of continuous intercalated pathways for ion transport, and this leads to the different interaction between the electrolyte, NGP and PANI materials.[41,25] Second, the content of functional groups on NGP/PANI films significantly influences the interfacial capacitance by introducing pseudocapacitance,[34] NGP/PANI with different weight ratios may play an synergistic role in determining the CV shapes and capacitance. Therefore, it is suggested that NGP/$PANI_{1:1.5}$ films exhibit the best capacitance due to the ideal synergistic combination of the conducting and mechanical properties of NGP and high pseudocapacitance of the PANI component.

Impedance spectroscopy is used to measure the internal resistances, charge transfer kinetics, and ion diffusion processes of NGP/PANI electrodes. **Figure 4**A shows the Nyquist plots of supercapacitors with NGP/PANI electrodes. The vertical shape at lower frequencies indicates a pure capacitive behavior, the more vertical the curve, the more closely the supercapacitor behaves as an ideal capacitor.[23] Equivalent series resistance (ESR) estimated from the intercept of the curve on the x-axis is about 0.2 Ω (Figure 4A inset). ESR measurement can be used to estimate the rate at which the supercapacitor can be charged/discharged, and it is an important factor in determining the power density of the device. Consequently, the maximum power density of the supercapacitor has been calculated according to the equation $P_{max} = V_{max}^2/4MR$, where V_{max} is the maximum voltage, R is the ESR and M is the mass of the two electrodes.[23] With a cell voltage of 1.0 V, the best performance of the supercapacitors measured in this series is for the NGP/$PANI_{1:1.5}$ thin film, which exhibits a high power density of 454 kW kg^{-1}, with energy density of 9.3 Wh kg^{-1} at a scan rate of 20 mV s^{-1}.

To further comfirm the merits of the NGP/PANI films as supercapacitor electrodes, tests on the galvanostatic charge-discharge properties of the supercapacitor are performed at a constant current density of 1 A/g, with two-electrode system.[38] As shown in Figure S8B, the resulting curves are not fully linear, and the observed sweep can be attributed to the pseudocapacitiance behavior. The specific capacitance is calculated according to the equation $C = 2I\Delta t/(m\Delta V)$, where I is the modulus of the applied discharge current, Δt is the discharging time period for the potential change ΔV, $\Delta V = V_{max} - 0.5V_{max}$, and m is the average mass of one electrode. Figure 4B shows the variation of specific capacitance with cycle lifetimes for the NGP and NGP/PANI supercapacitor. After 1000 cycles, the specific capacitances for NGP, NGP/$PANI_{1:0.5}$, NGP/$PANI_{1:1}$, NGP/$PANI_{1:1.5}$ and NGP/$PANI_{1:2}$ are 26.8, 80, 186, 352, 197 F g^{-1}. The high specific capacitance values for NGP/PANI still persist after 1000 cycles, highlighting their good electrochemical stability.

Adv. Energy Mater. **2013**,
DOI: 10.1002/aenm.201300184

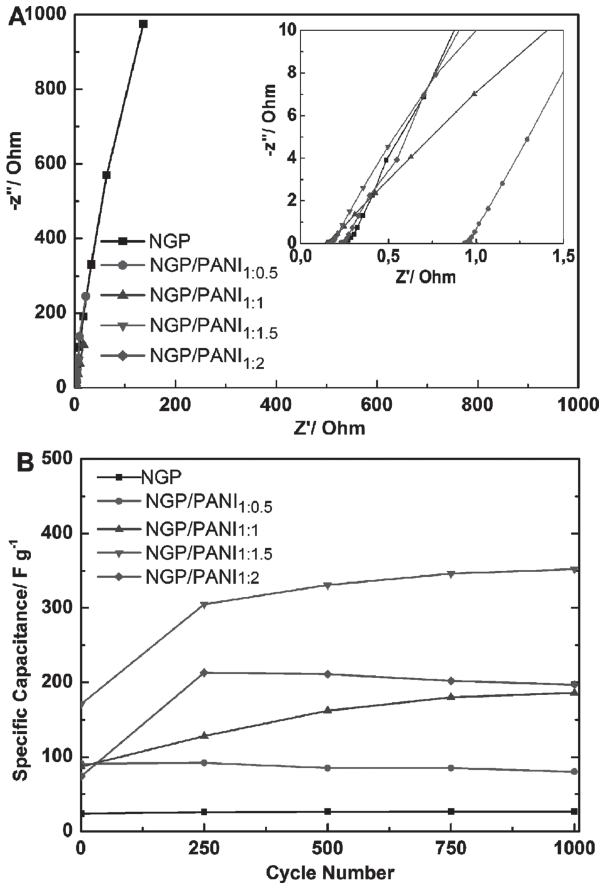

Figure 4. A) Nyquist plots of NGP and NGP/PANI supercapacitor device. Inset shows an enlarged scale. B) Cycling stability of the supercapacitor device over 1000 cycles, cycling stability measured at a constant current density of 1 A/g, with 1M H_2SO_4 electrolyte.

The combination of high NGP conductivity along with PANI reversible redox properties is regarded as necessary to achieve supercapacitors with long cycle-life.

An interesting phenomenon is observed with $NGP/PANI_{1:1.5}$ and $NGP/PANI_{1:1}$ where the specific capacitance improves significantly with increasing cycle number (Figure 4B). This phenomenon is reported previously for a NH_2-RG-O/PANi composite.[35] In our case, the capacitance increase is possibly due to the doping and dedoping of hydrogen sulfate ions (HSO_4^{-1}) on the PANI assisted by the simultaneous fast Faradic reactions of primary amine with H^+. The doping and dedoping of ions during the oxidation and reduction of PANI is responsible for the pseudocapacitive charge generation in these supercapacitors.[35]

To further demonstrate the mechanical robustness of the screen printed supercapacitor electrodes, we printed the $NGP/PANI_{1:1.5}$ ink on a flexible carbon substrates (Figure S3B), and prepared a bendable supercapacitor prototype by lamination (**Figure 5**A). Remarkbly, the $NGP/PANI_{1:1.5}$ supercapacitors show excellent mechanical integrity without any sign of delamination after the intentional bending (Figure 5B). This good mechanical integrity can be attributed to the high mechanical strength of NGP, and the good adhesion between the ink and the substrate. Figure 5C shows the flexible supercapcitor CV curves before, during, and after bending to a radius of 2.5 cm. Bending-unbending cycling measurements cause an increase in the capacitance up to 200 cycles. It can be possibly related to a cycling measurement induced improvement in the surface wetting of the electrode, leading to more electroactive surface area.[42] The capacitance performance of bending status is lower than that of flat status, which may be attributed to the difficulty in charge transfer caused by the relative poor conductivity of bending NGP/PANI films.[31] The supercapacitor performance is 146 F g^{-1} after 200 bending cycles. The peak position difference in the CV between the bent and flat status is still unkown. This performance of NGP/PANI flexible films shows them to be valuable candidates for the manufacture of flexible energy storage devices in "printed electronics".

In summary, printable NGP/PANI inks have been formulated successfully and a rapid and scalable screen printing technique has been used to prepare active electrodes for the supercapacitor devices. In two-electrode measurements, the supercapacitors containing electrodes of $NGP/PANI_{1:1.5}$ show the best specific capacitance of 269 F g^{-1}, power density of 454 kW kg^{-1} and energy density of 9.3 Wh kg^{-1}, operating in 1M H_2SO_4 electrolytes. The supercapacitor shows excellent cycling stability with no degradation over 1000 charge/discharge cycles. Moreover, the performance of the $NGP/PANI_{1:1.5}$ flexible supercapacitors are well-retained over 200 bending cycles. The key result of this work is the applicability of cheap and abundant raw materials

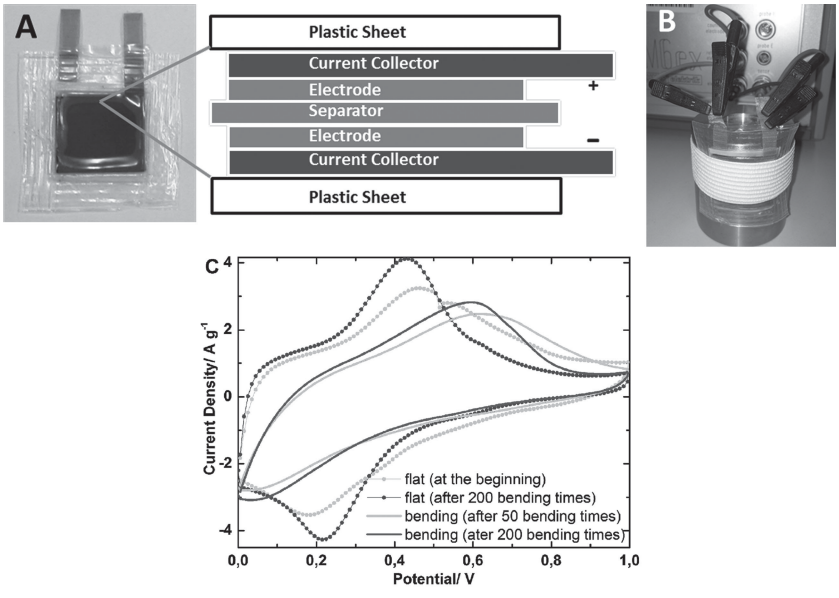

Figure 5. A) An optical image of an flexible supercapacitor device assembled in this work and schematic diagram of this device. B) An optical image of the flexible supercapacitor on the bending status. C) CV curves of the $NGP/PANI_{1:1.5}$ flexible electrode before, during, and after bending to a radius of 2.5 cm.

(NGP and PANI) used, the ink formulation processes and screen printing technology in the production of NGP/PANI thin film electrodes for use in supercapacitor devices on an industrial levels. These results pave the way for the fully-printable industrial supercapacitor application in the future.

Experimental Section

Ink Formulation: A series of homogenous NGP and NGP/PANI inks are prepared by ball milling method. The weight ratio of NGP, PANI and PTFE is varied as 90:0:10, 60:30:10, 45:45:10, 36:54:10, 30:60:10. And the resulting inks are labeled as NGP, NGP/$PANI_{1:0.5}$, NGP/$PANI_{1:1}$, NGP/$PANI_{1:1.5}$, NGP/$PANI_{1:2}$, respectively. Typically, for the ink labeled as NGP/$PANI_{1:1.5}$, ethanol (200 mL), milling ball (130 mL) and NGP powder (2.13 g) are added to capsule. The mixture is then placed under the shearing forces at a speed of 5500 rpm (14.4 m/s, ca. 100–150 watt, bead diameter 0.8–1.2 mm) for 1 hour, at 10 °C.

After this process, PANI (3.23 g) is added to the above mixture, and ball milling is carried out for 10 minutes at a speed of 5500 rpm, at 10 °C. Finally, PTFE (1 g, 60% in water) is added; again, ball milling is carried out for another 10 minutes at a speed of 5500 rpm, at 10 °C. The NGP/$PANI_{1:1.5}$ ink is then obtained. Other inks are made by varying the weight accordingly.

Viscosity Measurement: In order to investigate the flow behavior of the inks, we perform rheological measurements using the rheometer and the cone-plate equipment. Flow curves are carried out by increasing the shear rate from 1 to 1000 s^{-1}. This enables us to determine the high and low shear viscosity regime of our samples.

BET measurement: Nitrogen adsorption and desorption isotherm measurements are carried out at 77 K with a Quantachrom Autosorb 6B analyzer. Before the measurements, the samples are dried for 2 h at 80 °C.

Supporting Information

Supporting Information is available from the Wiley Online Library or from the author.

Acknowledgements

The authors would like to thank Thomas Kolb, and Waldemar Bartuli for supercapacitor measurements and valuable discussions. This work is financially supported by a Marie-Curie Fellowship within the frame of the GENIUS project (FP7 - PEOPLE Programme).

Received: February 19, 2013
Revised: March 12, 2013
Published online:

[1] M. Armand, J. M.Tarascon, *Nature* **2008**, *451*, 652.
[2] M. Berggren, D. Nilsson, N. D. Robinson, *Nat. Mater.* **2007**, *6*, 3.
[3] H. Yan, Z. H. Chen, Y. Zheng, C. Newman, J. R. Quinn, F. Dotz, M. Kastler, A. Facchetti, *Nature* **2009**, *457*, 679.
[4] F. C. Krebs, *Sol. Energy Mater. Sol. Cells* **2009**, *93*, 394.
[5] D. A. Pardo, G. E. Jabbour, N. Peyghambarian, *Adv. Mater.* **2000**, *12*, 1249.
[6] P. G. Bruce, S. A. Freunberger, L. J. Hardwick, J. M. Tarascon, *Nat. Mater.* **2012**, *11*, 19.
[7] M. Kaempgen, C. K. Chan, J. Ma, Y. Cui, G. Gruner, *Nano Lett.* **2009**, *9*, 1872.
[8] Y. Gogotsi, P. Simon, *Science* **2011**, *334*, 917.
[9] X. Ji, P. Hallam, S. Houssein, R. Kadara, L. Lang, C. Banks, *RSC Adv.* **2012**, *2*, 1508.
[10] F. Krebs, M. Jorgensen, K. Norrman, O. Hagemann, J. Alstrup, T. Nielsen, J. Fyenbo, K. Larsen, J. Kristensen, *Sol. Energy Mater. Sol. Cells* **2009**, *93*, 422.
[11] P. Simon, Y. Gogotsi, *Nat. Mater.* **2008**, *7*, 845.
[12] M. D. Stoller, S. J. Park, Y. Zhu, J. An, R. S. Ruoff, *Nano Lett.* **2008**, *8*, 3498.
[13] Y. Huang, J. Liang, Y. Chen, *Small* **2012**, *8*, 1805
[14] Z. Wu, A. Winter, L. Chen, Y. Sun, A. Turchanin, X. Feng, K. Müllen, *Adv. Mater.* **2012**, *24*, 5130.
[15] S. Pang, Y. Hernandez, X. Feng; K. Mullen, *Adv. Mater.* **2011**, *23*, 2779.
[16] Y. Zhu, S. Murali, M. D. Stoller, K. J. Ganesh, W. Cai, P. J. Ferreira, A. Pirkle, R. M. Wallace, K. A. Cychosz, M. Thommes, D. Su, E. A. Stach, R. S. Ruoff, *Science* **2011**, *332*, 1537.
[17] M. F. El-Kady, V. Strong, S. Dubin, R. B. Kaner, *Science* **2012**, *335*, 1326.
[18] Y. Zhu, S. Murali, W. Cai, X. Li, J. W. Suk, J. R. Potts, R. S. Ruoff, *Adv. Mater.* **2010**, *22*, 3906.
[19] C. Liu, Z. Yu, D. Neff, A. Zhamu, B. Z. Jang, *Nano Lett.* **2010**, *10*, 4863.
[20] B. Z. Jang, A. Zhamu, United States Patents 2010, US2010056819A.
[21] B. Z. Jang, A. Zhamu, United States Patent 2010, US2010055025A.
[22] Z. Yu, D. Neff, C. Liu, B. Jang, A. Zhamu, United States Patents 2012, US2012026643.
[23] Y. Wang, Z. Shi, Y. Huang, Y. Ma, C. Wang, M. Chen, Y. Chen, *J. Phys. Chem. C* **2009**, *113*, 13103.
[24] J. Zhang, X. Zhao, *J. Phys. Chem. C* **2012**, *116*, 5420.
[25] K. Zhang, L. Zhang; X Zhao, J. Wu, *Chem. Mater.* **2010**, *22*, 1392.
[26] L. Nyholm, G. Nystrom, A. Mihranyan, M. Stromme, *Adv. Mater.* **2011**, *23*, 3751.
[27] H. Bai, C. Li, G. Shi, *Adv. Mater.* **2011**, *23*, 1089.
[28] K. F. Kelly, W. E. Billups, *Acc. Chem. Res.* **2013**, *46*, 4.
[29] M. C. Hsiao, S. Liao, M. Y. Yen, P. Liu, N. W. Pu, C. Wang, C. Ma, *ACS Appl. Mater. Interfaces* **2010**, *2*, 3092.
[30] D. Tobjork, R. Osterbacka, *Adv. Mater.* **2011**, *23*, 1935.
[31] J. An, J. Liu, Y. Zhou, H. Zhao, Y. Ma, M. Li, M. Yu, S. Li, *J. Phys. Chem. C* **2012**, *116*, 19699.
[32] N. A. Kumar, H. J. Choi, Y. R. Shin, D. W. Chang, L. M. Dai, J. B. Baek, *ACS Nano* **2012**, *6*, 1715.
[33] D. Wang, F. Li, J. Zhao, W. Ren, Z. Chen, J. Tan, Z. Wu, I. Gentle, G. Lu, H. Cheng, *ACS Nano* **2009**, *3*, 1745.
[34] H. Wang, Q. Hao, X. Yang, L. Lu, X. Wang, *ACS Appl. Mater. Interfaces* **2010**, *2*, 821.
[35] L. Lai, H. Yang, L. Wang, B. Teh, J. Zhong, H. Chou, L. Chen, W. Chen, Z. Shen, R. Ruoff, J. Lin, *ACS Nano* **2012**, *6*, 5941.
[36] Z. Wen, X. Wang, S. Mao, Z. Bo, H. Kim, S. Cui, G. Lu, X. Feng, J. Chen, *Adv. Mater.* **2012**, *24*, 5610.
[37] X. Dong, H. Xu, X. Wang, Y. Huang, M. B. Chan-Park, H. Zhang, L. Wang, W. Huang, P. Chen, *ACS Nano* **2012**, *6*, 3206.
[38] M. Stoller, R. Ruoff, *Energy Environ. Sci.* **2010**, *3*, 1294.
[39] G. Yu, ; L. Hu,; N. Liu, H. Wang, M. Vosgueritchian, Y. Yang, Y. Cui, Z. Bao, *Nano Lett.* **2011**, *11*, 4438.
[40] Q. Wu, ; Y. Xu, Z. Yao, A. Liu, G. Shi, *ACS Nano* **2010**, *4*, 1963.
[41] A. Sarker, J. Hong, *Langmuir* **2012**, *28*, 12637.
[42] H. Wang, C. Holt, Z. Li, X. H. Tan, B. S. Amirkhiz, Z. Xu, B. Olsen, T. Stephenson, D. Mitlin, *Nano Res* **2012**, *5*, 605.